

## THE INNER RADIUS OF T TAURI DISKS ESTIMATED FROM NEAR-INFRARED INTERFEROMETRY: THE IMPORTANCE OF SCATTERED LIGHT.

PINTE, C.<sup>1</sup>, MÉNARD, F., BERGER, J.P., BENISTY, M., MALBET, F.

Laboratoire d'Astrophysique de Grenoble, CNRS/Université Joseph-Fourier, UMR 5571, B.P. 53, F-38041 Grenoble Cedex 9, France

*Draft version October 30, 2018*

### ABSTRACT

For young Herbig AeBe stars, near-infrared interferometric measurements have revealed a correlation between the luminosity of the central object and the position of the disk inner rim. This correlation breaks down for the cooler T Tauri stars, a fact often interpreted in terms of disks with larger inner radii. In most cases, the conversion between the observed interferometric visibility and the calculated disk inner radius was done with a crude disk emission model. Here, we examine how the use of models that neglect scattered light can lead to an overestimation of the disk sizes. To do so, synthetic disk images (and visibilities) are calculated with a full treatment of the radiative transfer. The relative contributions of thermal emission and scattered light are compared. We find that the latter can not be neglected for cool stars. For further comparison, the model visibilities are also converted into inner disk radii using the same simple disk models as found in the literature. We find that reliable inner radii can only be estimated for Herbig Ae/Be stars with these models. However, they lead to a systematic overestimation of the disk size, by a factor of 2 to 3, for T Tauri stars. We suggest that including scattered light in the models is a simple (and sufficient) explanation of the current interferometric measurements of T Tauri stars.

*Subject headings:* radiative transfer, scattering, techniques: interferometry, planetary systems: protoplanetary disks

### 1. INTRODUCTION

Near-infrared (NIR) broad-band interferometric observations of young stellar objects trace the inner part of the warm dusty circumstellar environment ( $\lesssim 1$  AU) and can be used to constrain its physical properties and to characterize the size and location of the emitting region.

The NIR sizes, derived from simple geometrical models, are found to be consistent with the dust sublimation radius for Herbig Ae and late Be objects (Monnier & Millan-Gabet 2002; Millan-Gabet et al. 2007 and references therein). Interestingly, observations of T Tauri stars reveal lower NIR visibilities (hereafter  $V^2$ ). They correspond to sizes larger than the dust sublimation radii when the same simple geometrical models are used (Akeson et al. 2005a; Eisner et al. 2005, 2007). Various explanations are proposed to account for these surprisingly low  $V^2$  (or large inner radii): extra heating from accretion, lower dust sublimation temperatures, small dust grains, photo-evaporation. As noted by Eisner et al. (2007), it is unlikely however that any of these mechanisms can explain by itself the large inner radii observed in all low mass T Tauri stars. Instead, Eisner et al. (2007) favor the explanation where the inner disk's position is controlled by the stellar magnetospheric pressure, in this case pushing the disk outward when accretion rates are low enough.

In this letter, we explore the possibility that the position of the inner disk is incorrectly estimated, especially for T Tauri stars, because the radiative transfer (hereafter RT) schemes used are incomplete, namely that the contribution from scattering is overlooked. Scattered light is a spatially extended component potentially leading to lower  $V^2$  and, by way of consequence, to a biased estimation of characteristic sizes when neglected. In the following, we investigate these ef-

fects, using detailed RT modelling, by comparing the spatial distribution of scattered light and thermal emission.

### 2. RADIATIVE TRANSFER MODELLING

Synthetic images are computed using the 3D radiative transfer code MCFOST (Pinte et al. 2006) at  $2.2 \mu\text{m}$  ( $K$  band), with a pixel sampling of  $0.125$  mas. The temperature structure is calculated assuming the dust is in radiative equilibrium with the local radiation field (including both the stellar and reprocessed contributions).  $K$  band maps are then computed by emitting and propagating the proper amount of stellar and disk thermal photon packets. All these packets are allowed to scatter in the disk as often as needed.

$V^2$  are calculated assuming a Gaussian field of view of  $50$  mas. This is the field of view of the Keck interferometer. A distance of  $140$  pc is used. We use these values for comparison with available data. We explore a range of stellar luminosities by varying the effective temperature from  $3000$  K to  $10000$  K, representing young stellar objects ranging from low mass T Tauri stars to Herbig Ae stars. The stellar radius is fixed at two solar radii and stars are assumed to radiate as blackbodies.

*Disk geometry.* — We adopt the same geometry as in Pinte et al. (2007), with a surface density  $\Sigma(r) = \Sigma_0 (r/r_0)^{-1}$ , a scale height  $h(r) = 10 (r/r_0)^{9/8}$  AU and  $r_0 = 100$  AU. The disk dust mass is set to  $10^{-4} M_\odot$  and the outer radius to  $300$  AU. The central part of the disk being optically thick, the inner radius ( $R_{\text{in}}$ ) is computed self-consistently, for each star, by moving it to the location where the dust temperature is equal to the dust sublimation temperature ( $T_{\text{sub}} = 1500$  K or  $2000$  K). At the inner edge, a radial Gaussian profile towards the central star, with a  $1/2e$  length of  $0.01 R_{\text{in}}$ , is used to reproduce a round-shaped inner rim, making it visible from all inclination angles. We restrict our analysis in this Letter to the pole-on case, without loss of generality as long as the

Electronic address: pinte@astro.ex.ac.uk

<sup>1</sup> School of Physics, University of Exeter, Stocker Road, Exeter EX4 4QL, United Kingdom

TABLE 1  
OPTICAL PROPERTIES AT  $2.2 \mu\text{m}$

Composition	$a_{\text{max}}$	albedo	$g^a$
A Silicates (Dorschner et al. 1995)	$1 \mu\text{m}$	0.90	0.53
B Silicates (Dorschner et al. 1995)	1 mm	0.80	0.62
C Si + C (Mathis & Whiffen 1989)	$1 \mu\text{m}$	0.37	0.58
D Si + C (Mathis & Whiffen 1989)	1 mm	0.62	0.91

<sup>a</sup>Asymmetry parameter,  $g = \langle \cos \theta \rangle$  with  $\theta$  the scattering angle

photosphere is directly visible by the observer.

*Dust properties.* — We consider homogeneous spherical grains with sizes distributed according to the power-law  $dn(a) \propto a^{-3.7} da$  between  $a_{\text{min}} = 0.03 \mu\text{m}$  and  $a_{\text{max}}$ . Because the relative contributions of scattered light and thermal emission will depend on the heating and scattering properties of dust, we explore various dust populations, by varying the maximum grain size  $a_{\text{max}} = 1 \mu\text{m}$  or 1 mm and the dust composition. Compact amorphous silicates grains (Dorschner et al. 1995) and a porous mixture of amorphous silicates and carbon (Mathis & Whiffen 1989, model A) are considered. Optical properties are calculated using Mie theory (Table 1) and the non-isotropic nature of the scattering is explicitly preserved in the calculations. A reference model (Silicates grains,  $a_{\text{max}} = 1 \mu\text{m}$ ,  $T_{\text{sub}} = 2000 \text{ K}$ ) is first discussed in sections 3.1, 3.2, 3.3 and the effects of the different dust properties are analysed in section 3.4.

### 3. RESULTS

#### 3.1. Brightness profiles

In this section we present the cumulative fluxes, integrated in a circular aperture, as a function of distance from the star. Each contribution, i.e., direct and scattered starlight and direct and scattered thermal emission from the disk, is plotted separately for comparison. Two models ( $T_{\text{eff}} = 10\,000 \text{ K}$ , upper panel and  $T_{\text{eff}} = 4\,000 \text{ K}$ , lower panel) are presented in Fig. 1.

For the  $T_{\text{eff}} = 10\,000 \text{ K}$  model, the sublimation radius is located at 0.40 AU from the star (3 mas at 140 pc). Because the disk is warm, the thermal emission is of the same order as the stellar emission at  $K$  band. All contributions (except the photosphere) show similar radial profiles. Because the disk is optically thick, the dominant contribution is the scattered thermal emission from the disk, i.e., the photons coming from deep inside the disk that had to scatter before reaching the surface. Depending on radius, this contribution is as large as 2.5 times the direct disk emission in  $K$  band because the emission volume is larger. This contribution is often neglected. Within a 50mas field-of-view, direct starlight is the next contributor to the total flux, followed by direct thermal emission from the disk. The scattered starlight contributes significantly less, of the order of a few % of the stellar flux. It is only a small fraction of the direct starlight because the stellar photosphere is seen directly and the disk is geometrically thin.

For the cooler star, the sublimation radius is located closer to the photosphere, down to 0.34 mas (0.048 AU). It is only marginally resolved by current interferometers. In this case, contrarily to the more massive star, scattered starlight is of the same order as thermal emission. It can even dominate at larger distances from the star. Such a difference comes from the fact that T Tauri stars radiate a larger fraction of their bolometric luminosity in the NIR and because the disk  $K$  band emitting zone is smaller (i.e., smaller inner radius and cooler disk). Then, because the direct thermal emission flux decreases faster with radius than scattered light, the integrated

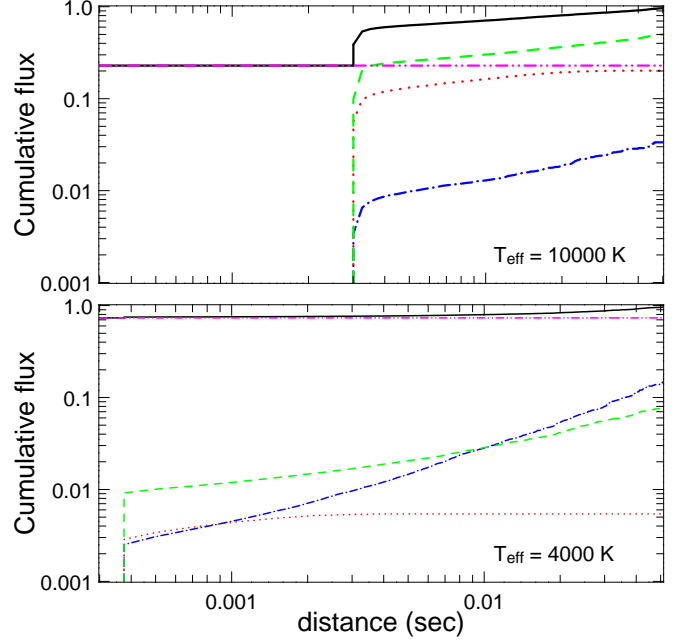


FIG. 1.—  $K$  band integrated fluxes for a 10 000 K star (upper panel) and 4 000 K star (lower panel) distant of 140 pc. Full black line : total flux, magenta dot-dot-dash: direct stellar light, blue dot-dashed: scattered stellar light, red dotted line: direct thermal emission, green dashed line : scattered thermal emission. The total flux is normalized to 1 at a distance of 50 mas. All contributions lead to a disk-to-stellar flux ratio of  $\approx 3.35$  and 0.37 for the 10 000 K and 4 000 K star respectively.

thermal emission curve increases more slowly than both scattered components (photospheric and disk thermal). A significant effect of scattered light on  $V^2$  is therefore expected.

#### 3.2. Visibilities

As shown in section 3.1, scattering can contribute significantly to the circumstellar flux, even at small scales. To evaluate the incidence of neglecting scattering in the interpretation of  $V^2$ , we compare two  $V^2$  curves in Fig. 2: i) direct Fourier transform of the images obtained through the MCFOST calculations (solid line), ii) Fourier transform of the image without any scattered light and where the thermal emission is scaled to the total infrared excess to compensate. This is as if all the total disk flux were emitted following the emission profile of the direct disk thermal emission (dashed line). It ensures that the disk-to-star flux ratio remains equal in both cases.

A comparison of both curves shows that  $V^2$  are similar at long baselines for the  $T_{\text{eff}} = 10\,000 \text{ K}$  star (Fig. 2, left panel). This is an indication that most of the emitting structure is in a small zone, at or close to the inner rim. However,  $V^2$  become different at baselines smaller than  $\sim 50 \text{ m}$ . Differences are of the order of a few percents for baselines shorter than 20 m where the large scale structure is completely resolved and contributes as uncoherent light, hence reducing the  $V^2$ .

$V^2$  computed by taking into account the spatial extension of scattered light are smaller than  $V^2$  computed assuming that all the disk excess comes from direct thermal emission. This is particularly striking for  $T_{\text{eff}} = 4\,000 \text{ K}$  (Fig. 2, right panel). In this case, the discrepancy between both  $V^2$  curves is dominated by the large scale structure of both photospheric and thermal scattered light. This large scale structure appears in the fast  $V^2$  drop of about 0.05 occurring on baselines shorter than  $\approx 20 \text{ m}$ . Since the object is less resolved because the inner disk rim is closer in, and because the contribution of large

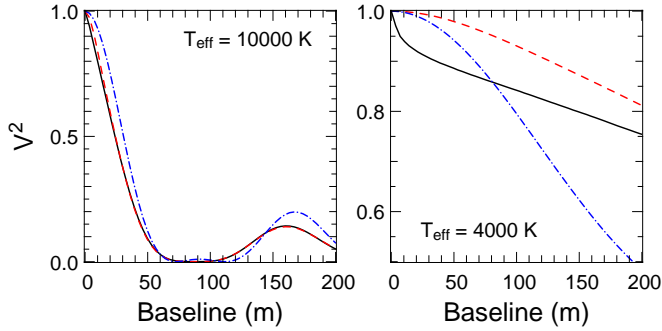


FIG. 2.—  $V^2$  curves. Left: Herbig Ae star with  $T_{\text{eff}} = 10\,000$  K. Right: T Tauri star,  $T_{\text{eff}} = 4\,000$  K. The full lines present the  $V^2$  obtained from MCFOST images and the dashed lines, the  $V^2$  calculated from the direct thermal emission only (but with same excess). The dot-dash lines show the  $V^2$  of the ring models which have been fitted on the  $V^2$  points at 80 m.

scale structures (scattered light) to the overall excess budget is larger than in the previous case, the discrepancy between the two curves is permanent throughout the whole baseline range. *Therefore, the interpretation of  $V^2$  measurements attributing all the excess emission to pure thermal emission is incorrect for cool stars and previous results must be taken with care.* In particular, since these measurements are often made with a precision of  $\approx 5\%$  they can lead to significant errors which are discussed in the following section.

### 3.3. Estimation of inner radii from NIR visibilities

The decrease of  $V^2$  at short baselines due to the larger spatial extent of scattered light can result in an overestimation of the inner radius of the disk if interpreted in the wrong context. To quantify this effect, we fit the  $V^2$  calculated above with a simple geometrical model composed of an unresolved point source surrounded by a thin ring, as done, e.g., by Akeson et al. (2005a) and Eisner et al. (2005, 2007). We adopt a Gaussian brightness profile in the radial direction<sup>2</sup>. The contribution (flux) of the ring is set to the total contribution (excess) from the disk (i.e., thermal emission + scattered light). As the models have been calculated for pole-on disks, we restrict the study to circular rings. Fitting is performed on *one*  $V^2$  point at a baseline of 80 m (the average projected baseline in the observations of Akeson et al. 2005a) and the resulting  $V^2$  curves are shown in Fig. 2 (dot-dash lines).

For the  $T_{\text{eff}} = 10\,000$  K star, this curve remains close to the  $V^2$  curve calculated with full RT, indicating that the derived radius (0.42 AU) is a good estimation of the actual inner radius (0.40 AU). However, at short baselines the shape of the curves differ significantly, with differences larger than 10% for a 20 m baseline. *Therefore, for warm stars, results from short baseline measurements should be taken with caution since they can be biased by extended emission (scattering).* Interestingly, such a decrease of  $V^2$  at short baselines have been observed for a few objects with IOTA (Monnier et al. 2006)<sup>3</sup>. Similarly, results from longer baselines and more distant objects (i.e. sampling the same spatial scales as described here) should also be interpreted with care.

For the cooler  $T_{\text{eff}} = 4\,000$  K star the situation is worse. The  $V^2$  curve fitted with a ring is no longer a good approximation of the true disk  $V^2$  curve because of very different be-

<sup>2</sup> The exact profile of the ring does not matter for our study, as long as the width of the ring is small compared to its radius.

<sup>3</sup> These observations were performed in the  $H$  band but the effect of scattered light is similar.

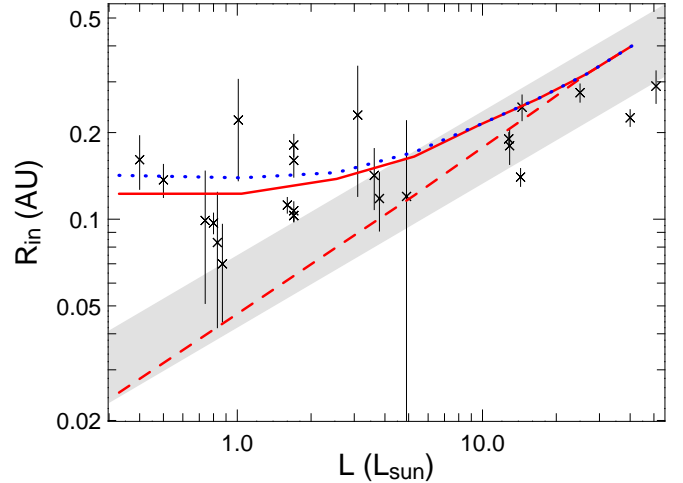


FIG. 3.— Comparison of the radius derived with a ring model (full line, field of view of 50 mas) with the (true) physical inner radius of the disk (dashed line) as the function of the stellar luminosity. The dotted line shows the radius derived assuming a field of view of  $1''$ . Crosses correspond to observational data points (see Table 2). We omit error bars on luminosity to avoid crowding. The shaded area shows the location of the sublimation radii calculated as in Eisner et al. (2007), for  $T_{\text{sub}}$  between 1 500 and 2 000 K. This represents the location of the size-luminosity diagram where most of the Herbig Ae stars lie. Note that the slope of sublimation radius is larger in our modelling because small grains ( $a_{\text{max}} = 1\ \mu\text{m}$ ) are used.

havior at short baselines. The inferred ring radius (0.12 AU) is in that case a large overestimation of the actual inner radius of the disk (0.048 AU).

Fig. 3 shows the derived ring size as a function of the stellar luminosity (full line), compared to the true sublimation radius (dashed line). When neglecting scattered light, *the ring size is always an overestimation of the actual inner disk radius* and this overestimation increases as the temperature of the central object decreases.

Radii estimated with ring models fitted on Keck interferometer observations are over-plotted on Fig. 3. The selected sources are CTTS and Herbig stars at a distance close to 140 pc and have been observed in  $K$  band (Table 2). Interestingly, the location of the fitted inner radii mimics very well the distribution of data points. Therefore, the contribution of scattered light appears as a simple and sufficient explanation of the observed trend of lower  $V^2$  seen in late type PMS stars given the current error bars on the measurements.

Not all data in the literature were obtained with the same instrument however. To estimate the effect of the interferometer's field of view, we plot on Fig. 3 the derived ring size for a field of view of  $1''$ , valid for the Palomar Testbed Interferometer for instance. As expected, the impact of scattered light is more pronounced, with a derived radius of 0.14 AU for  $T_{\text{eff}} = 4\,000$  K and is increasing with decreasing stellar temperature. However, because the brightness of scattered light decreases rapidly with distance from the star, the effect remains limited and significantly smaller than the one resulting from the contribution inside the inner 50 mas.

### 3.4. Effect of dust properties

In order to test the dependence of the findings presented in section 3.3 on dust properties, Fig. 4 shows the derived radii for several dust populations. The general behavior remains unchanged and the effect of scattered light on  $V^2$  is significant for all dust populations we treated.

However, finer differences may be linked to the dust properties. First, the position of the inner rim depends on the dust

TABLE 2  
SELECTED SOURCES

Name	distance	L ( $L_{\odot}$ )	$R_{\text{ring}}$ (AU)	Reference
CI Tau	140 pc	0.8	$0.097 \pm 0.008$	1
DK Tau A	140 pc	1.7	$0.103 \pm 0.005$	1
DK Tau A	140 pc	1.7	$0.107 \pm 0.008$	1
DK Tau B	140 pc	0.5	$0.137 \pm 0.018$	1
RW Aur A	140 pc	1.7	$0.103 \pm 0.005$	1
RW Aur A	140 pc	1.7	$0.181 \pm 0.016$	1
RW Aur B	140 pc	0.4	$0.161 \pm 0.034$	1
V1002 Sco	160 pc	3.8	$0.118 \pm 0.027$	1
AS 206	160 pc	1.6	$0.112 \pm 0.007$	1
BP Tau	140 pc	0.83	$0.083 \pm 0.041$	2
DG Tau	140 pc	3.62	$0.142 \pm 0.034$	2
GM Aur	140 pc	1.01	$0.221 \pm 0.085$	2
LkCa15	140 pc	0.74	$0.099 \pm 0.048$	2
RW Aur	140 pc	1.7	$0.160 \pm 0.020$	2
AS 207A	160 pc	3.1	$0.23 \pm 0.11$	3
V2508 Oph	160 pc	4.9	$0.12 \pm 0.10$	3
SA 205A	160 pc	14.3	$0.14 \pm 0.01$	3
MWC 758	150 pc	$25 \pm 4$	$0.275 \pm 0.02$	4
HD 144432	145 pc	$14.5 \pm 4$	$0.245 \pm 0.025$	4
HD 150193	150 pc	$51 \pm 17$	$0.29 \pm 0.075$	4
MWC 275	122 pc	$40 \pm 8$	$0.225 \pm 0.015$	4

REFERENCES: 1, Eisner et al. (2007) ; 2, Akeson et al. (2005a) ; 3, Eisner et al. (2005) ; 4, Monnier et al. (2005).

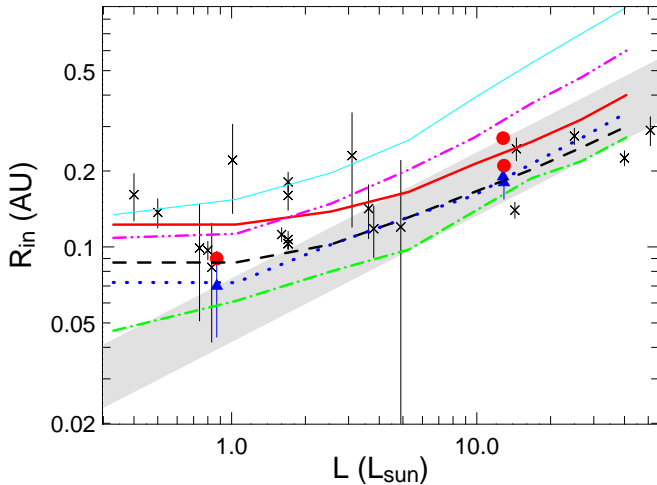


FIG. 4.— Measured inner radii as a function of the stellar luminosity for different dust populations: dust model A (red full line), B (black dashed line), C (blue dotted line), D (green dot-dashed line) with  $T_{\text{sub}} = 2000$  K and dust models A (cyan thin full line) and B (pink dot-dot-dashed line) with  $T_{\text{sub}} = 1500$  K. Crosses are observations from literature, blue triangle and red circles are the sizes derived by Akeson et al. (2005b) with ring models and RT models respectively.

properties. The effect is to shift the curves vertically on Fig. 4. Smaller grains and silicates are more efficiently heated and the corresponding sublimation radius is increased. Similarly, different materials with smaller sublimation temperatures also result in larger inner radii. Second, because of different scattering properties (albedo and phase function), the fraction of scattered light is larger for silicates grains, and so is the ratio of the measured radius over the actual inner radius.

Silicates dust, models A and B, provides a good match to the data, although we have not explored all possibilities. Intermediate dust properties should also agree with the data points.

Moreover, with the density structure we adopted, resulting in very opaque central regions, a sublimation temperature of 1500 K yields inner radii that are too large to reproduce the observed trend at high luminosity (shaded region).

Interestingly, detailed modelling of PTI interferometric observations has been performed by Akeson et al. (2005b), including light scattering. The authors concluded that RT models have similar radii than geometrical models. They use dust properties with an albedo of 0.5,  $g = 0.6$  (intermediate to our dust properties C and D),  $T_{\text{sub}} = 1600$  K and their less luminous source (DR Tau) has a luminosity of  $0.87 L_{\odot}$ . With similar parameters, we do indeed find that the overestimation of the inner radius remains limited (about 30-40%), in agreement with the results of Akeson et al. (2005b) who found a difference of  $\approx 30\%$  for DR Tau between RT and ring models (see triangles and circles in Fig. 4). Unfortunately, this result was used as a validation for all sources. Should they have used different dust properties or considered lower luminosity sources, the discrepancy between the two methods would have been more striking. Because the effect of scattered light is systematic (always a decrease of  $V^2$ ) and always larger than 30% with respect to ring models, i.e. larger than observational error bars, we suggest that scattered light should always be included in the analysis of NIR  $V^2$ : the cooler the object the more needed scattered light is.

#### 4. CONCLUSIONS

We have investigated the effect of a complete treatment of RT in the interpretation of  $V^2$ . We find scattered light is an important contribution to the disk excess and dominates for low luminosity/cool objects. In particular, we have shown this contribution to lead to a systematic decrease of the observed  $V^2$ . *Interpreted in the wrong context, the lower  $V^2$  can be mistaken with disks of larger inner radii.* For more luminous objects ( $> 20 L_{\odot}$ ), the effect becomes significant only at short baselines ( $< 20$  m) but care must also be taken.

Depending on the adopted dust properties, part, if not all of the observed trend of estimated large radii of late type objects can be explained by the contribution of scattered light, without requiring any other mechanism than dust sublimation to truncate the inner disk.

However, there are several issues to consider to estimate quantitatively the exact position of the inner boundary of a given disk. The dust properties have an impact on the actual location of the disk sublimation radius and on the fraction of scattered light sent to the observer. Since the dust properties are not known accurately, the position of the sublimation radius remains slightly uncertain. Additional effects, like viscous heating as part of the accretion process for example, might also lead to a different disk temperature profile, hence to a different emission profile. A more detailed case by case modelling effort together with additional constraints from other observations, such as mid-infrared spectroscopy or spectro-interferometry, should be of great help to overcome these degeneracies.

#### REFERENCES

Akeson, R. L., Boden, A. F., Monnier, J. D., et al. 2005a, ApJ, 635, 1173  
Akeson, R. L., Walker, C. H., Wood, K., et al. 2005b, ApJ, 622, 440

Dorschner, J., Begemann, B., Henning, T., Jaeger, C., & Mutschke, H. 1995, A&A, 300, 503

Eisner, J. A., Hillenbrand, L. A., White, R. J., Akeson, R. L., & Sargent, A. I. 2005, *ApJ*, 623, 952  
Eisner, J. A., Hillenbrand, L. A., White, R. J., et al. 2007, *ArXiv e-prints*, 707  
Mathis, J. S. & Whiffen, G. 1989, *ApJ*, 341, 808  
Millan-Gabet, R., Malbet, F., Akeson, R., et al. 2007, 539  
Monnier, J. D., Berger, J.-P., Millan-Gabet, R., et al. 2006, *ApJ*, 647, 444

Monnier, J. D. & Millan-Gabet, R. 2002, *ApJ*, 579, 694  
Monnier, J. D., Millan-Gabet, R., Billmeier, R., et al. 2005, *ApJ*, 624, 832  
Pinte, C., Fouchet, L., Ménard, F., Gonzalez, J.-F., & Duchêne, G. 2007, *A&A*, 469, 963  
Pinte, C., Ménard, F., Duchêne, G., & Bastien, P. 2006, *A&A*, 459, 797